

DYNAMICS OF COMPANION GALAXIES OF EARLY-TYPE GALAXIES

CHENG-YU CHEN¹ AND CHORNG-YUAN HWANG¹

¹*Graduate Institute of Astronomy, National Central University, Zhongli, Taiwan 32001*

Submitted to ApJ

ABSTRACT

We estimated the dynamical masses of 115 early-type galaxies (ETGs) by analyzing the dynamics of satellite and companion galaxies of these ETGs. We selected galaxies with absolute magnitudes between -22 and -25 in the K_s -band from the Extragalactic Distance Database (EDD). We also selected 216 spiral galaxies for comparison. We employed a simple model to simulate the observed dynamical mass from satellite galaxies at various distances. Our simulations showed that the dynamical masses derived from satellite galaxies with elliptical orbits would be smaller than those with circular orbits even they contain the same dark mass halos. Therefore, relationships between the observed M_{dyn}/M_b distributions and distances would depend on orbital shapes. From the relationships between our observed M_{dyn}/M_b distributions and distances, we suggest that the satellite galaxies of the ETGs have relatively more elliptical orbits than those of the spiral galaxies have and the M_{dyn}/M_b of the ETGs are greater than that of the spiral galaxies.

Keywords: Early-type galaxies — Galaxy dark matter halos — Galaxy evolution

arXiv:2009.05788v1 [astro-ph.GA] 12 Sep 2020

1. INTRODUCTION

The existence of dark matter phenomena has been known for more than 50 years. These phenomena were first detected from flat rotation curves in spiral galaxies (Zwicky 1937; Rubin & Ford 1970; Roberts & Whitehurst 1975; Corbelli & Salucci 2000). Flat rotation curves suggest that invisible mass in the outer part is producing additional gravitational force. Several studies have proposed that dark matter is the dominant source of mass in spiral galaxies (Ostriker & Peebles 1973; Faber & Gallagher 1979; Corbelli & Salucci 2000; Sofue 2012).

Early-type galaxies (ETGs) have different evolution channels related to mass (Cappellari 2016; Penoyre et al. 2017; Li et al. 2018). Dwarf ETGs might form from ram-pressure stripping (Toloba et al. 2011) or gas accretion of dwarf spiral galaxies (Graham et al. 2017; Janz et al. 2017). Normal ETGs ($M_* \leq 2 \times 10^{11} M_\odot$) could form from major mergers of spiral galaxies (Cox et al. 2006; Penoyre et al. 2017) or star formation quench after the bulge growing up (Martig et al. 2009; Cappellari 2016). High-mass ETGs ($M_* \geq 2 \times 10^{11} M_\odot$) might form from dry mergers of low-mass ETGs (Bell et al. 2006; Cappellari 2016; Penoyre et al. 2017; Li et al. 2018) or major mergers of spiral galaxies (Bois et al. 2010). ETGs are expected to contain a large amount of dark matter remaining from progenitor spiral galaxies. However, several studies have revealed that visible matter is dominated in the inner regions of ETGs; for example, Sanders (2014) found that there are 65 elliptical galaxies showing little or no dark matter. Moreover, several other studies also discovered that individual ETGs possess little dark matter in their inner regions (Romanowsky et al. 2003; van de Ven et al. 2010; Ruff et al. 2011; Lane et al. 2015; Nigoche-Netro et al. 2015; Boardman et al. 2016; Jin et al. 2020). Conversely, Wojtak & Mamon (2013) discovered that red galaxies have more concentrated dark halos relative to blue galaxies. The phenomenon of little dark matter in some individual ETGs may be due to the nonexistence of dark matter (Sanders 2014), galaxy evolution or the spatial distribution of dark matter. Dekel et al. (2005) simulated the merging process and concluded that the low-velocity dispersions observed in the study by Romanowsky et al. (2003) were due to the radial orbits of halo stars. Dark matter might have different distributions for different galaxies. For example, dark matter were expected to follow the Navarro-Frenk-White (NFW) model (Navarro et al. 1996) (or other distribution models), whereas baryon matter of ETGs and spiral galaxies may follow the deprojected de Vaucouleurs' model and the exponential model, respectively. These models may have different effective radii and cause variance in dark matter ratios at different radii (Courteau & Dutton 2015). On the other hand, several studies have revealed that dark matter is dominated in the outer region of ETGs via globular cluster kinematics (Forbes et al. 2016; Alabi et al. 2016, 2017) or satellite galaxy dynamics (e.g. McKay et al. 2002; More et al. 2011; Wojtak & Mamon 2013; Lange et al. 2019).

Satellite galaxy dynamics have been analyzed in many studies to measure the dark matter abundance on halo scales. McKay et al. (2002) analyzed 618 isolated galaxies surrounded by 1225 faint satellite galaxies in the Sloan Digital Sky Survey (SDSS) and concluded that the halo masses and central galaxy luminosities correlated linearly. Brainerd & Specian (2003) tested the relation described by McKay et al. (2002) using satellite kinematics in the Two-Degree Field Galaxy Redshift Survey (2dFGRS); the study showed that for the spiral host, the halo mass is independent of the central luminosity. Prada et al. (2003) also analyzed the satellite dynamics of isolated galaxies in the SDSS and concluded that the line-of-sight velocity dispersions of satellite galaxies decreased with the distance to the central galaxies and that the decline is consistent with the predictions of cosmo-

logical models. Prada et al. (2003) also found that the relation between satellite velocity dispersions and central absolute magnitudes is very close to the Tully-Fisher relation for normal spiral galaxies. Conroy et al. (2007) analyzed satellite dynamics by combining data from the DEEP2 Galaxy Redshift Survey and the SDSS and found that the red central galaxies have more massive halo masses than blue central galaxies for fixed luminosity. More et al. (2011) also used the SDSS to analyze satellite dynamics and found that red hosts have more massive halos than blue hosts for the same luminosity, and that there is no significant difference in the average halo mass of the red and blue hosts with the same stellar mass. Lange et al. (2019) analyzed satellite kinematics using the seventh data release (DR7) of the SDSS and observed that red central galaxies have more massive halos than blue ones of the same luminosity, and the halo mass is correlated with the average luminosity of the central galaxies.

In this study, we analyzed the dynamics of satellite galaxies of ETGs to derive the total dark matter associated with ETGs and compared these dynamics with those of spiral galaxies. Our data selection process is described in Section 2. We derive the dynamical masses of ETGs and compare them with those of spiral galaxies in Section 3. Finally, we discuss the implications of mass distribution for galaxy evolution and summarize the findings of our study in Section 4. The Hubble constant adopted in this study is $H_0 = 70 \text{ km s}^{-1} \text{ Mpc}^{-1}$.

2. DATA

We selected our galaxy samples from the Extragalactic Distance Database (EDD; Tully et al. 2009). The EDD contains tables from various sources, including the Updated Nearby Galaxy Catalog (Karachentsev et al. 2013), the galaxy group catalog of the Two Micron All Sky Survey (2MASSGC; Tully 2015), the third edition of the Cosmicflows database (Tully et al. 2016), and the Arecibo Legacy Fast ALFA HI catalog (Haynes et al. 2018). We obtained the K_s -band magnitudes and distances from EDD. Galaxies in the local universe (less than 50 Mpc) were selected so that their small satellite galaxies could be observed (i.e. M_{K_s} brighter than -21.7 at 50 Mpc corresponding to the limiting magnitude of the 2MASSGC ≈ 11.75). We used galaxies with absolute magnitudes between -22 and -25 in the K_s -band as our host galaxy samples. We considered galaxies with a distance of less than 250 kpc from a host galaxy as neighboring galaxies and selected systems that had only one neighboring galaxy to avoid groups or clusters of galaxies. Spiral galaxies and their companion galaxies with the same criteria were also selected for comparison. We obtained the morphological types of these galaxies from the NASA/IPAC Extragalactic Database. We did not select any mergers or irregular galaxies in the host galaxy and companion galaxy samples to avoid strong interacting galaxies. The minimum projected distance between the host galaxies and companion galaxies was approximately 16 kpc.

We considered the baryonic mass $M_b = L_K \times M/L_K + M_g$, where L_k is the luminosity of the K_s -band, M/L_K is the stellar mass-to-light ratio in the K_s -band, and M_g is the gas mass. Gavazzi et al. (1996) used 928 spiral galaxies from eight clusters with distances between 11 and 110 Mpc and noted that near-infrared M/L_K was almost constant. Bell et al. (2003) estimated the stellar mass functions of galaxies in the local universe using a ‘diet’ Salpeter initial mass function (IMF) and reported that $M/L_K = 0.95 \pm 0.03$ and that most of the stellar mass in the local Universe is in ETGs. McGaugh & Schombert (2014) studied the color M/L relation of disk galaxies in the local universe using four population synthesis models (Bell et al. 2003; Portinari et al. 2004; Zibetti et al. 2009; Into & Portinari 2013), which were assumed a scaled Salpeter IMF, Kroupa (1998) IMF, Chabrier

(2003) IMF, and Kroupa IMF, respectively; the four models were revised for self-consistency, and the study reported $M/L_K \approx 0.6$. We adopted stellar $M/L_K = 0.95$ and 0.6 for our ETG and spiral galaxy samples, respectively.

The gas mass was estimated using $M_g = 1.33[M(\text{HI}) + M(\text{H}_2)]$, where the factor of 1.33 was due to the helium abundance (Boselli et al. 2014; McGaugh, & Schombert 2015). The HI mass was obtained from the 21-cm flux using $M(\text{HI}) = 2.36 \times 10^5 D^2 \text{flux}(\text{HI})$ (McGaugh, & Schombert 2015). The H_2 masses of some galaxies were obtained from literature (Young et al. 1989; Kennicutt et al. 2003; Kuno et al. 2007; Leroy et al. 2008). For the galaxies without available H_2 mass, we used the relationship between $M(\text{H}_2)$ and $M(\text{HI})$ described by Boselli et al. (2014) to obtain the molecular gas mass. For the ETGs, the atomic and molecular gas contents are much smaller than the stellar mass, and the different molecular mass estimates do not affect the final M_{dyn}/M_b . For the spiral galaxies, the atomic gas content is usually less than 30% of the stellar mass, and the molecular gas content is 30% of the atomic gas on an average (Boselli et al. 2014); therefore, the different molecular mass estimates can only cause a difference of a few percent in the final M_{dyn}/M_b value.

We determined the dynamical mass from the relative velocity of the companion galaxy in the line of sight. In the random distribution, the true velocity v of a galaxy is related to the line-of-sight velocity v_{los} by the equation $v^2 = 3v_{\text{los}}^2$. Therefore, the dynamical mass is related to the line-of-sight velocity as $GM_{\text{dyn}}/d = 3v_{\text{los}}^2$, where G is the gravitational constant, d is the projected radius between the host galaxy and the neighboring galaxy, and v_{los} is the relative velocity of the companion galaxy on the line of sight. The formula used for estimating dynamical mass is based on an idealized case. The distance between a companion and host galaxy is larger than the radius of each galaxy. The mass of the host galaxy within the satellite galaxy's orbit can thus be considered a point source at the center of the host galaxy if no dark halo surrounds the host galaxy. However, if a dark matter halo surrounds the galaxy, our method can be used to estimate the dark matter up to the distance between a companion and host galaxy if the dark halo is spherically symmetric. Therefore, the derived results are unaffected by the shape, rotation, or brightness profiles of the host galaxies (Campbell et al. 2017; Nigoche-Netro et al. 2019).

The results might be affected by the inclination angles of the orbits of satellite galaxies. However, for numerous galaxies, the viewing angles are uniformly distributed in the 3D space. Therefore, the M_{dyn}/M_b distributions measured are affected only by the real M_{dyn}/M_b value. If the observed M_{dyn}/M_b distributions of ETGs are similar to the distributions of spiral galaxies, the real M_{dyn}/M_b of ETGs and spiral galaxies should be similar to each other. Dark matter constitutes approximately 90% of the total mass in spiral galaxies (Rubin 1983; Khalil & Muñoz 2002; Courteau et al. 2014; Di Paolo et al. 2019). We assumed that the upper limit of the dark matter fraction of ETGs is 90%; therefore, for a galaxy containing 90% dark mass, $M_{\text{dyn}}/M_b = 30$ was the maximum value of the formula used to determine dynamical mass (Equation A3). We then only selected the galaxies that were considered to be gravitationally bounded, namely those in which $M_{\text{dyn}} < 30M_b$, to be our final samples. Our final samples comprised 115 ETGs and 216 spiral galaxies. However, the chosen cutoff point might affect the final results. We discuss the effects of using various cutoff points in Section 4.

3. RESULT

We analyzed the dynamical masses of ETGs and compared them with those of spiral galaxies. Figure 1 displays the distributions of the dynamical-to-baryonic mass ratio M_{dyn}/M_b of both ETGs and spiral galaxies. We then used the Kolmogorov-Smirnov (K-S) test to determine whether the two

$M_{\text{dyn}}/M_{\text{b}}$ ratios were from the same population. The results revealed a 39% chance of indistinguishable distribution of $M_{\text{dyn}}/M_{\text{b}}$ between the ETGs and spiral galaxy samples, which indicated a similar $M_{\text{dyn}}/M_{\text{b}}$ of ETGs and spiral galaxies.

Our galaxy samples had absolute magnitudes between -22 and -25. We compared the $M_{\text{dyn}}/M_{\text{b}}$ distribution of galaxies between different magnitude ranges to investigate the relation between luminosity and dynamical mass. Figure 2 displays the $M_{\text{dyn}}/M_{\text{b}}$ distributions of galaxies with different absolute magnitudes. The K-S test results of these distributions have p -value > 0.05 and indicate that the $M_{\text{dyn}}/M_{\text{b}}$ distributions of galaxies with different absolute magnitudes were indistinguishable.

We analyzed the $M_{\text{dyn}}/M_{\text{b}}$ values estimated at various distances to investigate the spatial distributions of dark matter. Figure 3 presents the $M_{\text{dyn}}/M_{\text{b}}$ distributions measured from the companion galaxies at different distances from the host galaxies for both morphologies. Table 1 lists the distribution results of the K-S test, which indicated that the $M_{\text{dyn}}/M_{\text{b}}$ distributions of closer and farther companion galaxies of the ETGs were not substantially different. However, the farther companion galaxies of spiral galaxies had larger $M_{\text{dyn}}/M_{\text{b}}$ values than the closer satellite galaxies of spiral galaxies. We also tested the correlation with Kendall's tau, which is a non-parametric measure of the correlation between two ranked parameters. The null hypothesis of Kendall's rank test is that the two parameters are independent. The τ and p -value for the ETGs are 0.013 and 0.84, respectively, whereas those for the spiral galaxies are 0.23 and 6.3×10^{-7} , respectively. These results also indicate that $M_{\text{dyn}}/M_{\text{b}}$ is not correlated with d for the ETGs but is correlated for the spiral galaxies.

4. DISCUSSION

We analyzed $M_{\text{dyn}}/M_{\text{b}}$ values from the dynamics of the early-type and spiral galaxy companions. Figure 1 revealed that the $M_{\text{dyn}}/M_{\text{b}}$ distributions of ETGs and spiral galaxies were similar; the K-S test indicates that the dark matter fractions in the outskirts of the ETGs were similar to those of the spiral galaxies. We also obtained the same conclusions from the 2-sample Anderson-Darling (A-D) test. The test statistic for the A-D test is 0.65, and the p -value is greater than 0.1. These results also indicate that the $M_{\text{dyn}}/M_{\text{b}}$ distributions of the ETGs and the spiral galaxies are indistinguishable.

We investigate the possible influence of the dark matter fraction cutoff on our results. We obtained the $M_{\text{dyn}}/M_{\text{b}}$ distributions by applying 80% and 95% dark matter fraction cutoffs, which correspond to $M_{\text{dyn}}/M_{\text{b}}$ distribution cutoffs of 15 and 60, respectively. Figure 4 illustrates the $M_{\text{dyn}}/M_{\text{b}}$ distributions obtained using various cutoff values. We then checked the similarity using the K-S and A-D tests. The p -values of the K-S test are 0.25 and 0.33 for 80% and 95% cutoffs, respectively, and the test statistics of the A-D test are 1.04 and 0.64 for 80% and 95% cutoff, respectively; both values correspond to p -values greater than 0.1. These results suggest that the $M_{\text{dyn}}/M_{\text{b}}$ distributions of the ETGs and the spiral galaxies are similarly independent of the cutoffs.

Figure 2 shows that the $M_{\text{dyn}}/M_{\text{b}}$ distributions are not related to luminosities. The brighter galaxies contain larger baryonic masses; therefore, the similar $M_{\text{dyn}}/M_{\text{b}}$ ratios indicate that the dark halos of the brighter galaxies are more massive. This result is in agreement with the positive correlation between the dark halo mass and the central galaxy luminosity, as described in previous works (McKay et al. 2002; Prada et al. 2003; Lange et al. 2019).

Figure 3 reveals that the $M_{\text{dyn}}/M_{\text{b}}$ values of ETGs were not related to the distances between the companion and host galaxies, whereas the $M_{\text{dyn}}/M_{\text{b}}$ values of the spiral galaxies were. For the ETG samples, the $M_{\text{dyn}}/M_{\text{b}}$ values measured from the closer and farther companions were indistinguishable. By contrast, the farther companion galaxies of spiral galaxies demonstrated larger $M_{\text{dyn}}/M_{\text{b}}$

values of the host galaxies than did the closer companions. These results may indicate different dark matter density profiles for the ETGs and spiral galaxies; in this situation, the dark matter of the ETGs galaxies would be more concentrated in the inner regions, whereas that of the spiral galaxies would be expanded to the outer regions. These results are consistent with those of [Wojtak & Mamon \(2013\)](#), who discovered that the dark matter halos of red host galaxies are significantly more concentrated than those of blue hosts of the same stellar mass are. Another possibility is that the orbits of the companion galaxies of the ETGs and spiral galaxies may have different degrees of ellipticity. We employed a simple model to simulate the observed dynamical masses from the satellite galaxies at different elliptical orbits. We assumed that all masses were distributed within 50 kpc, and the pericenter to apocenter length ratios ϵ of the orbits were 0.2, 0.4, 0.6, 0.8, and 1. The details of our simulations are described in Appendix A. The simulated results are presented in Figure 5. The satellite galaxies with circular or nearly circular orbits exhibited considerable dynamicsdistance relations; farther satellites exhibited larger M_{dyn}/M_b values of the host galaxies than closer satellites. However, the satellite galaxies with more elliptical orbits did not exhibit a dynamicsdistance relationship. These results indicated that the orbits of the companion galaxies of the ETG samples may be more elongated than those of the spiral galaxies. [Wojtak & Mamon \(2013\)](#) also found that satellite orbits around red galaxies are radial anisotropic and that satellite orbits around blue galaxies are consistent with isotropic models. The reason behind this elongation can be understood by considering the merger of a system with two host galaxies and a satellite galaxy. When the two host galaxies merge, most of the angular momentum of the system will be passed to the satellite galaxy. The satellite galaxy will gain angular momentum from the progenitor galaxies during the merging process and will follow an elongated orbit surrounding the merged ETG. This process is dynamically similar to the encounters between binaries and single stars; during the encounter, the two more massive stars are tightly bound, and the third one is ejected ([Hills 1975](#)). Similar process was reported by [Dekel et al. \(2005\)](#), who simulated disk-galaxy mergers and found that the orbits of the outer stars of resulting galaxies were elongated. Since the M_{dyn}/M_b values measured from elongated orbits are smaller than those from circular orbits with the same real M_{dyn}/M_b , the similar M_{dyn}/M_b distributions from observation data indicate that the ETGs have larger real M_{dyn}/M_b than the spirals. These result are consistent to some previous studies, which suggested that red host galaxies had more massive halos than blue ones with the same optical magnitudes ([Conroy et al. 2007](#); [More et al. 2011](#); [Lange et al. 2019](#)). Although our host galaxies were classified based on morphologies, our ETG sample is redder than the spiral one as shown in Figure 6.

Our model mainly considers the influence of the orbital anisotropies of satellite galaxies. The anisotropic effects originate primarily from the viewing angles and orbital shapes. We measured more than 100 galaxies; the probability that we observed all of these galaxies at certain viewing angles is negligible. Therefore, the influence of viewing angles on the orbits of the satellite galaxies is minimized. On the other hand, we would underestimate the dynamical mass of the host galaxies by considering satellite galaxies with elongated elliptical orbits. Figure 5 also illustrates the M_{dyn}/M_b distribution measured from satellite galaxies with different orbital shapes and shows that the M_{dyn}/M_b distribution is skewed toward lower M_{dyn}/M_b for more elongated orbits.

We also used the method of [McKay et al. \(2002\)](#) to derive the dynamical mass within 250 kpc of the host galaxies, M_{250}^{dyn} , for comparison to verify consistency between our method and others. We

used the spherical Jeans equation to determine the dynamical mass (Binney & Tremaine 2008),

$$\frac{GM(r)}{r} = -\overline{v_t^2} \left[\frac{d \log n(r)}{d \log r} + \frac{d \log \overline{v_r^2}}{d \log r} + 2\beta \right], \quad (1)$$

where r is the 250 kpc radius to which we integrate the mass, $\overline{v_r^2}$ is the radial mean square velocity, $n(r)$ is the number density of satellites as a function of radius, and β is the velocity anisotropy $\beta = 1 - \overline{v_t^2}/\overline{v_r^2}$. We assumed that the radial mean squared velocity $\overline{v_r^2}$ is equal to the line-of-sight mean squared velocity $\overline{v_{\text{los}}^2}$ as McKay et al. (2002) did, who found that $\overline{v_{\text{los}}^2} = 1.03 \pm 0.03 \overline{v_r^2}$. We then determined the number densities and mean square velocities for various distances between the companion and host galaxies. Subsequently, we fitted the data to the linear relation between log number density and log distance and to the linear relation between log mean square velocity in apertures from 50 to 250 kpc and log distance. The value of $\frac{d \log n(r)}{d \log r}$ is the slope of the fitted line of the density profile–distance relation, and the value of $\frac{d \log \overline{v_r^2}}{d \log r}$ is the slope of the velocity profile–distance relation. We found that the values of $\frac{d \log n(r)}{d \log r}$ are -2.2 and -2.3 for the ETGs and the spiral galaxies, respectively, and those of $\frac{d \log \overline{v_r^2}}{d \log r}$ are -0.49 and -0.11 for the ETGs and the spiral galaxies, respectively. The anisotropy values are usually between 0 and 0.5 (Prada et al. 2003; Wojtak & Mamon 2013; Lange et al. 2019); therefore, we use the anisotropy values $\beta = 0, 0.25, \text{ and } 0.5$. These results are shown in Figure 7. The M_{250}^{dyn}/M_b values of the ETGs were greater than those of the spiral galaxies. These results ostensibly differed from the results presented in Figure 1. However, our simulations indicated that, on average, satellites of ETGs follow more elliptical orbits than those of spiral galaxies do. This suggests that our method potentially underestimated the dynamical masses of the ETGs. Therefore, ETGs, on average, have greater dynamical-to-baryonic mass ratios than spiral galaxies have. Thus, the results derived from our method are consistent with those obtained from applying the method of McKay et al. (2002). We note that the M_{250}^{dyn}/M_b values obtained from Equation 1 are much larger than the M_{dyn}/M_b values obtained using the method described in Section 2. The main reason for this is that in Equation 1, the dynamical mass is estimated for the total halo mass within 250 kpc, but our method provides an estimate of the halo mass only within the projected distances for individual galaxies. The projected distances of individual galaxies are usually much smaller than 250 kpc; smaller M_{dyn}/M_b values are thus derived. Furthermore, our data differed from the data of McKay et al. (2002), who have selected galaxy sample up to $500 h^{-1}$ kpc, and we thus obtained a different mean square velocity profile and different $\frac{d \log \overline{v_r^2}}{d \log r}$ value. However, this difference in $\frac{d \log \overline{v_r^2}}{d \log r}$ values negligibly affected on the results. Even when we substituted $\frac{d \log \overline{v_r^2}}{d \log r}$ with 0 as McKay et al. (2002) did, the M_{250}^{dyn}/M_b values of our ETGs remained larger than those of the spiral galaxies in our sample, and the results did not change.

Figure 8 shows a comparison of our results to the results of More et al. (2011) and Wojtak & Mamon (2013). Our results show similar trends to their results but have smaller dynamical-to-stellar mass ratios. The main reason of the difference is likely that we only selected satellite galaxies within 250 kpc of the host galaxies whereas More et al. (2011) and Wojtak & Mamon (2013) selected satellites within at least 400 kpc of their host galaxies. We note that the mass in More et al. (2011) and Wojtak & Mamon (2013) was derived for the mass within 200 times of the critical density. The difference of the derived dark matter mass is mainly caused by the different adopted halo sizes.

We assumed constant stellar M/L ratios to obtain stellar masses. The luminous mass was dependent on several factors, mainly on the brightness profile and initial mass function (IMF) used to obtain the M/L ratio (Chen et al. 2010; Cappellari et al. 2012, 2013; Emsellem et al. 2014; Nigoche-Netro et al. 2015, 2016, 2019). We adopted the relationship between stellar mass and luminosity proposed by Lim et al. (2017, hereafter L17) to test the possible effects of these factors. The L17 stellar mass and luminosity were obtained from the Evolution and Assembly of GaLaxies and their Environments (EAGLE) simulation (Schaye et al. 2015; Crain et al. 2015; McAlpine et al. 2016), which adopts the Chabrier (2003) IMF and the spectral synthesis model of Bruzual, & Charlot (2003) to obtain stellar masses and luminosities, respectively. The relation is given by

$$\log M = 5.42 \times 10^{-2} \exp(0.376 \log L) + 7.31.$$

This formula was obtained by fitting the published data of L17. The masses and luminosities are in units of $M_{\odot}h^{-2}$ and $L_{\odot}h^{-2}$, respectively, and we assumed $h = 0.7$. Figure 9 displays the $M_{\text{dyn}}/M_{\text{b}}$ distributions of both ETGs and spiral galaxies with the L17 M/L relationship. The K-S test result revealed a 50% chance of indistinguishable distribution. We also repeated our analysis for Figures 2 and 3 using the L17 M/L relationship; the results are illustrated in Figures 10 and 11. The K-S test of the distributions is displayed in Table 2, which indicate that the results illustrated in Figures 10 and 11 are similar to those displayed in Figure 2 and 3. These findings suggest that the similarity in $M_{\text{dyn}}/M_{\text{b}}$ ratios between ETGs and spiral galaxies were not affected by differences in luminous mass estimates.

In this study, we compared the dynamics of the companion galaxies of ETGs and spiral galaxies. Our results revealed that first, ETGs have higher dynamical-to-baryonic mass ratios than spiral galaxies have at the same baryonic mass. Second, satellites of ETGs tend to follow more elliptical orbits than satellites of spiral galaxies do. We noted that these conclusions were derived statistically and may not apply to individual galaxies.

This work is supported by the Ministry of Science and Technology of Taiwan (grants MOST 107-2119-M-008-009-MY3). This research has made use of the NASA/IPAC Extragalactic Database (NED), which is operated by the Jet Propulsion Laboratory, California Institute of Technology, under contract with the National Aeronautics and Space Administration.

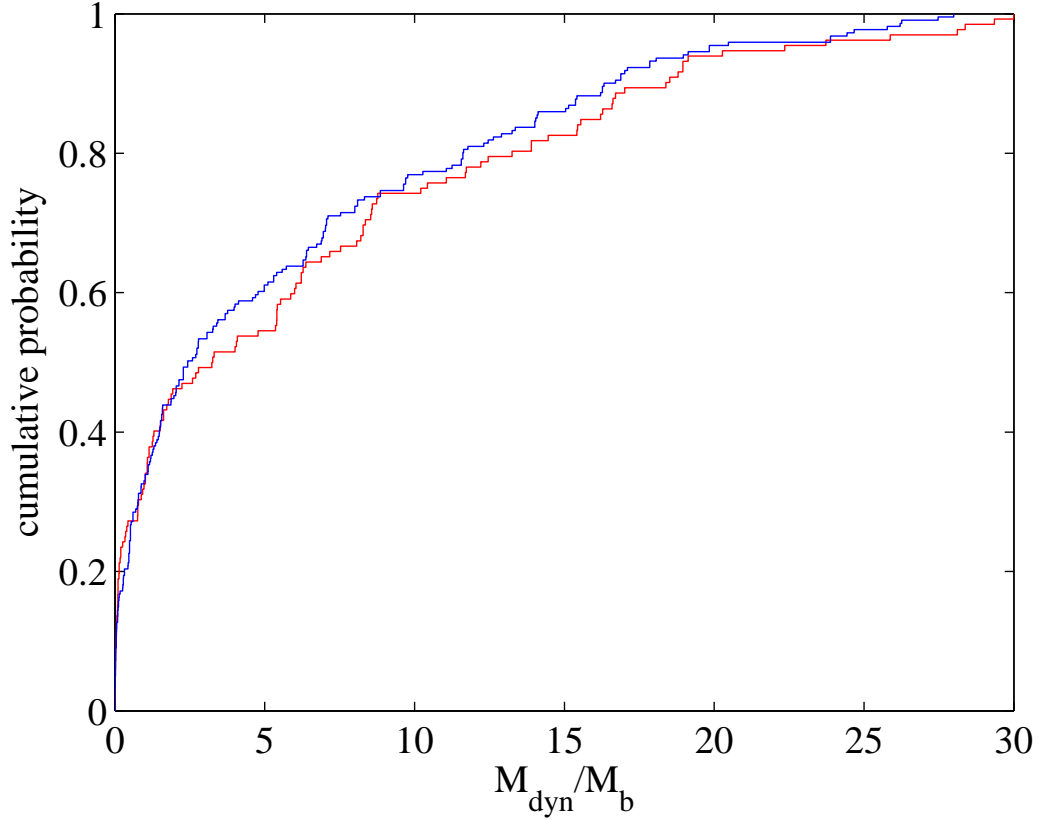


Figure 1. Probability distributions of M_{dyn}/M_b of ETGs and spiral galaxies. The red and blue lines represent the distributions of the ETGs and spiral galaxies, respectively.

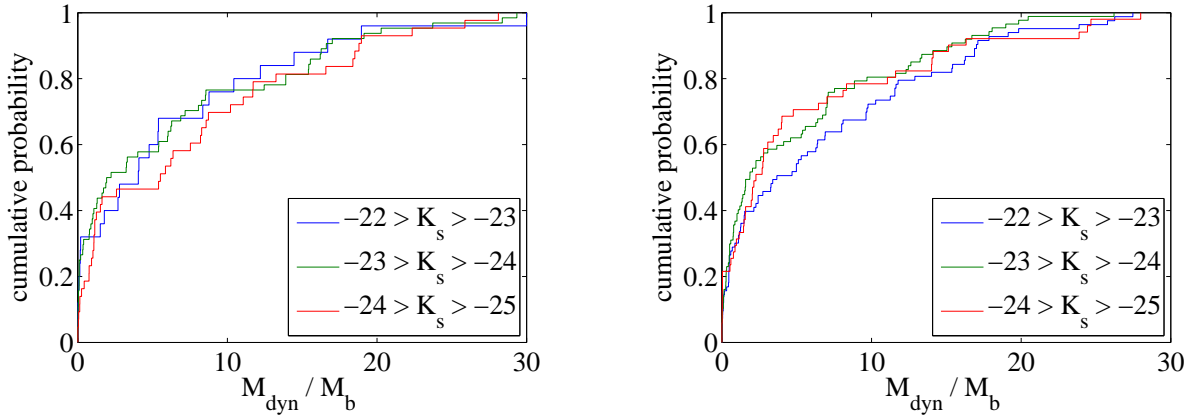


Figure 2. Probability distributions of M_{dyn}/M_b of the ETGs and spiral galaxies of different galaxy luminosities. Left: M_{dyn}/M_b of ETGs. Right: M_{dyn}/M_b of spiral galaxies. The blue, green, and red lines represent the M_{dyn}/M_b distributions of the galaxies that had absolute magnitudes from -22 to -23, -23 to -24, and -24 to -25, respectively.

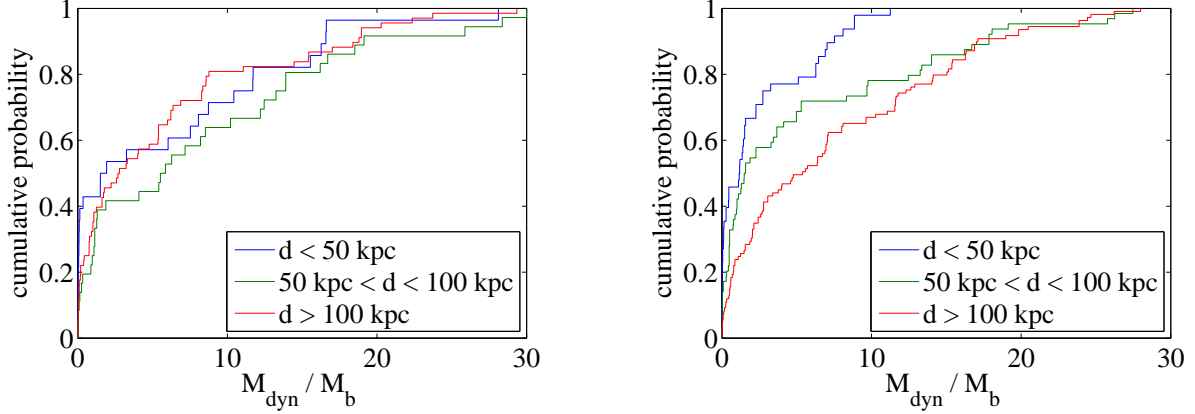


Figure 3. Probability distributions of M_{dyn}/M_b of the ETGs and spiral galaxies of different observed satellite-to-host galaxy distances. Left: M_{dyn}/M_b of ETGs. Right: M_{dyn}/M_b of spiral galaxies. The blue, green, and red lines represent the M_{dyn}/M_b distributions for distances less than 50 kpc, between 50 kpc and 100 kpc, and greater than 100 kpc, respectively.

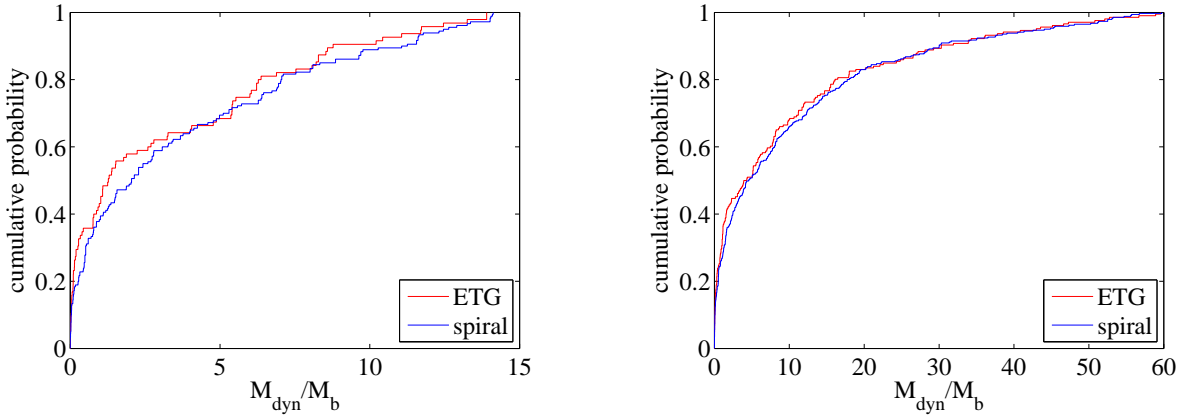


Figure 4. Probability distributions of M_{dyn}/M_b of the ETGs and spiral galaxies using 80% and 95% dark matter fraction cutoff. Left: 80% dark matter fraction cutoff. Right: 95% dark matter fraction cutoff. The red and blue lines represent the M_{dyn}/M_b distributions of ETGs and spiral galaxies, respectively.

Table 1. Probabilities of the K-S test of M_{dyn}/M_b in various observed satellite-to-host galaxy distances.

| | ETGs | | spiral | |
|--------------------------|--------------|--------------------------|--------------|--------------------------|
| | $d < 50$ kpc | 50 kpc $< d < 100$ kpc | $d < 50$ kpc | 50 kpc $< d < 100$ kpc |
| 50 kpc $< d < 100$ kpc | 20% | – | 4.6% | – |
| $d > 100$ kpc | 35% | 64% | 0.19% | 2.4% |

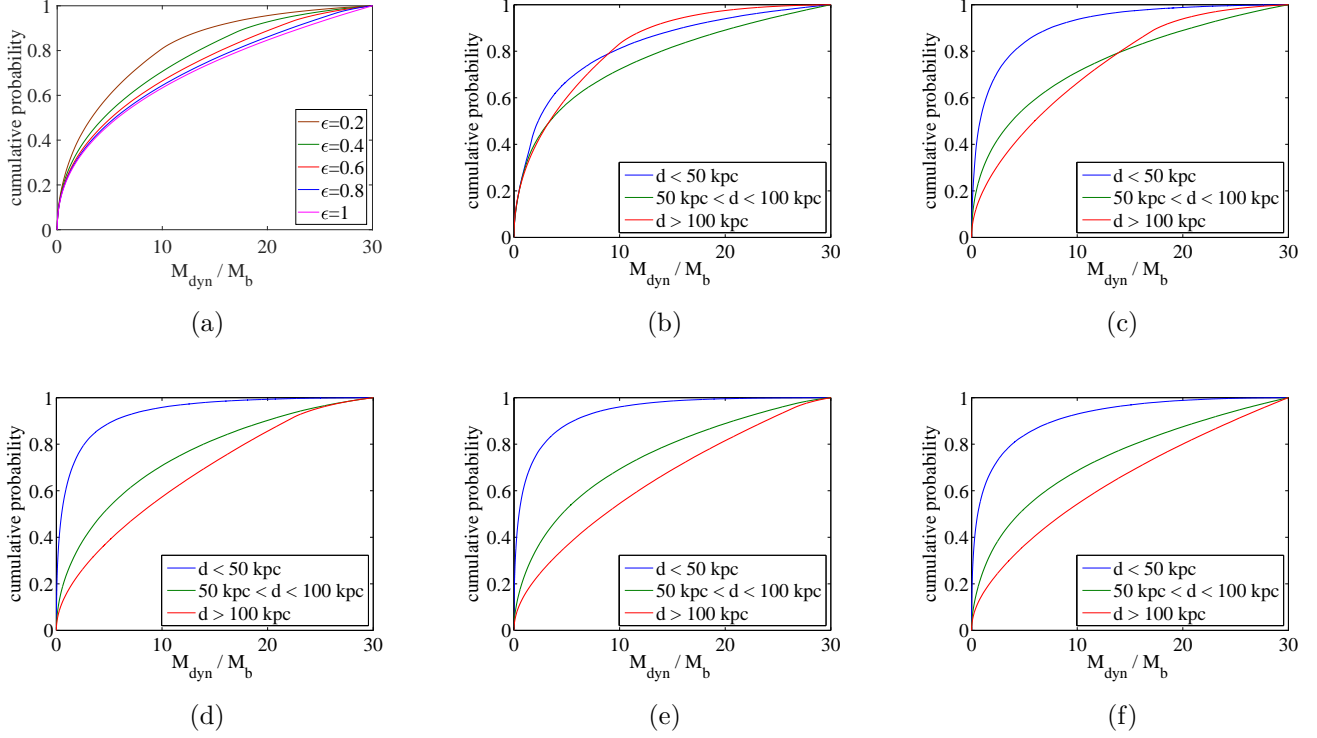


Figure 5. Probability distributions of simulated M_{dyn}/M_b values for different elliptical orbits. (a) Brown, green, red, blue, and magenta lines represent the results for the orbits with pericenter to apocenter length ratios (ϵ) of 0.2, 0.4, 0.6, 0.8, and 1, respectively. (b-f) The M_{dyn}/M_b distributions of different observed satellite-to-host galaxy distances for orbit with ϵ values of (b) 0.2, (c) 0.4, (d) 0.6, (e) 0.8 and (f) 1, respectively. Blue, green, and red lines represent the results for distances less than 50 kpc, between 50 kpc and 100 kpc, and greater than 100 kpc, respectively.

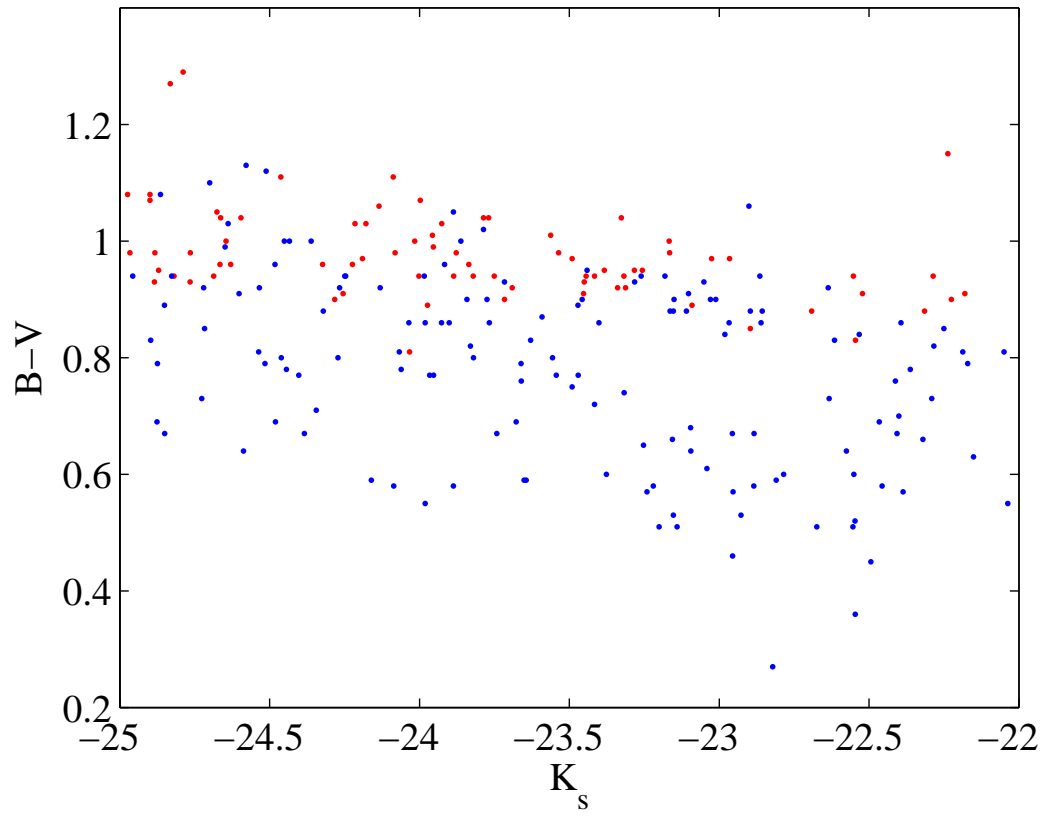


Figure 6. Color-Magnitude diagram of the host galaxies. The red and blue dots represent the distributions of the ETGs and spiral galaxies, respectively.

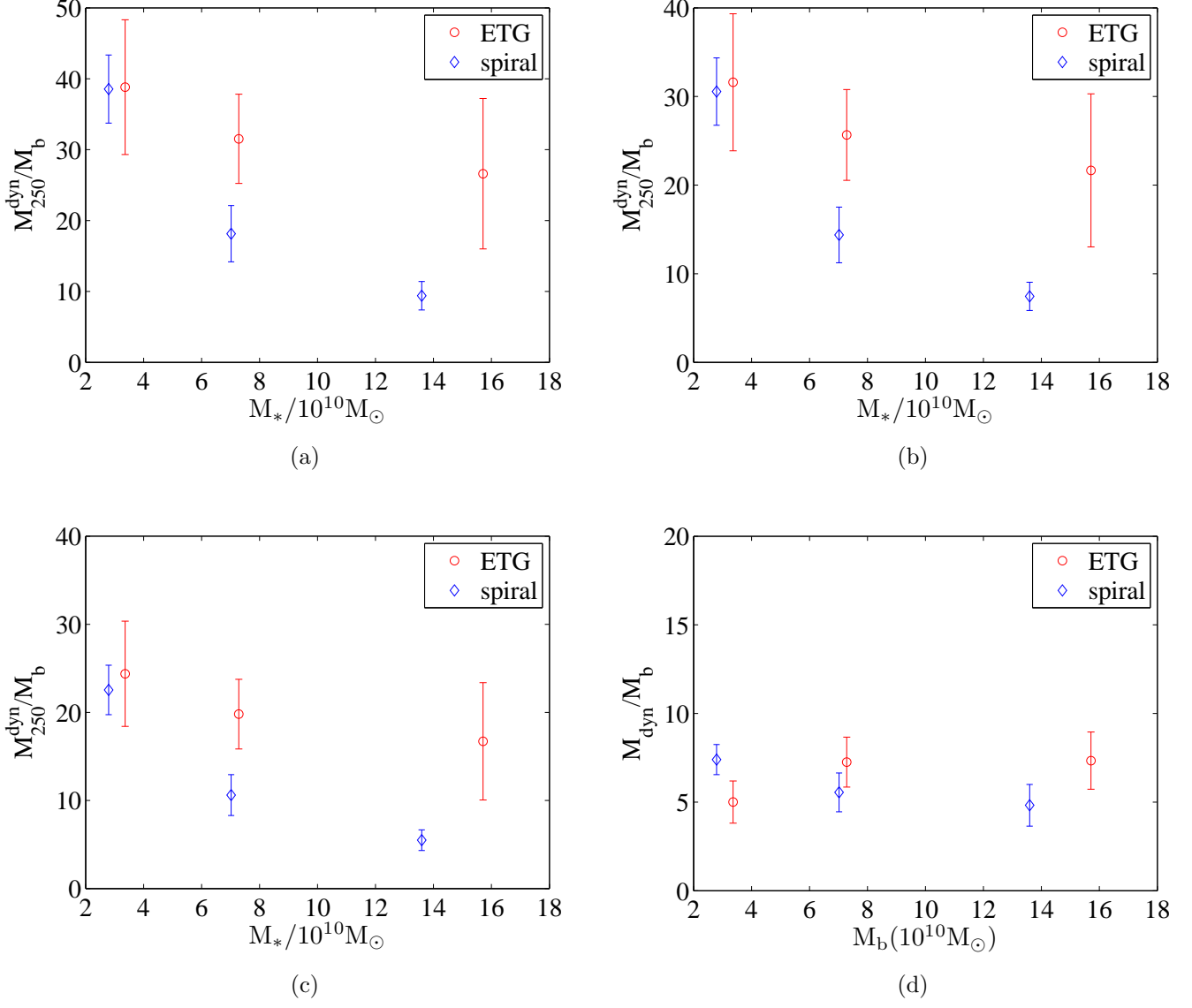


Figure 7. M_{250}^{dyn}/M_b as a function of baryon mass with various anisotropy values (a) $\beta = 0$ (b) $\beta = 0.25$, and (c) $\beta = 0.5$. The results derived from our statistical method are shown in (d) for comparison. The galaxy samples were divided into three baryonic mass bins: $M_b < 5 \times 10^{10}M_\odot$, $5 \times 10^{10}M_\odot < M_b < 10 \times 10^{10}M_\odot$, and $M_b > 10 \times 10^{10}M_\odot$.

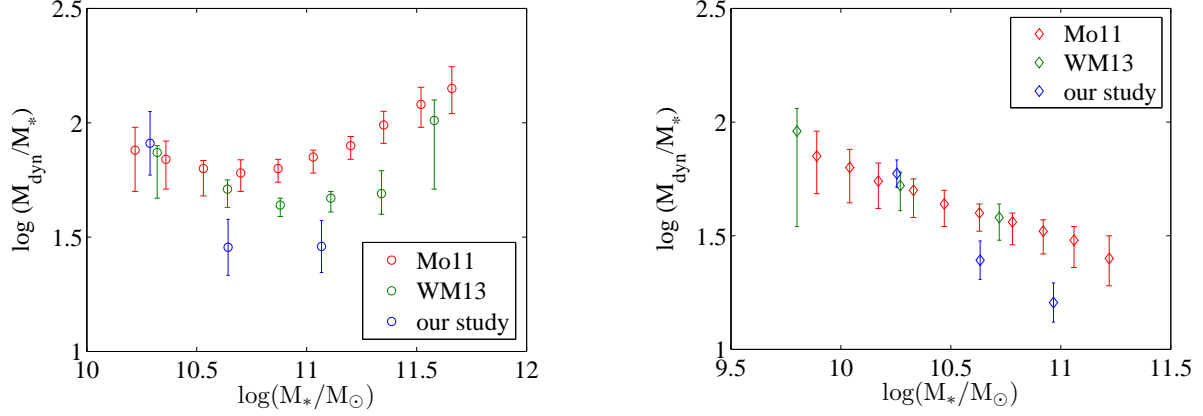


Figure 8. Dynamical-to-stellar mass ratios as a function of stellar mass. Left: ETGs of our study (blue) and red hosts of *More et al. (2011, Mo11, red)* and *Wojtak & Mamon (2013, WM13, green)*. Right: spirals of our study (blue) and blue hosts of *More et al. (2011, Mo11, red)* and *Wojtak & Mamon (2013, WM13, green)*. $\beta = 0$ was assumed for our study in this figure. Please note that the mass in *More et al. (2011)* and *Wojtak & Mamon (2013)* was derived for the mass within 200 times of the critical density.

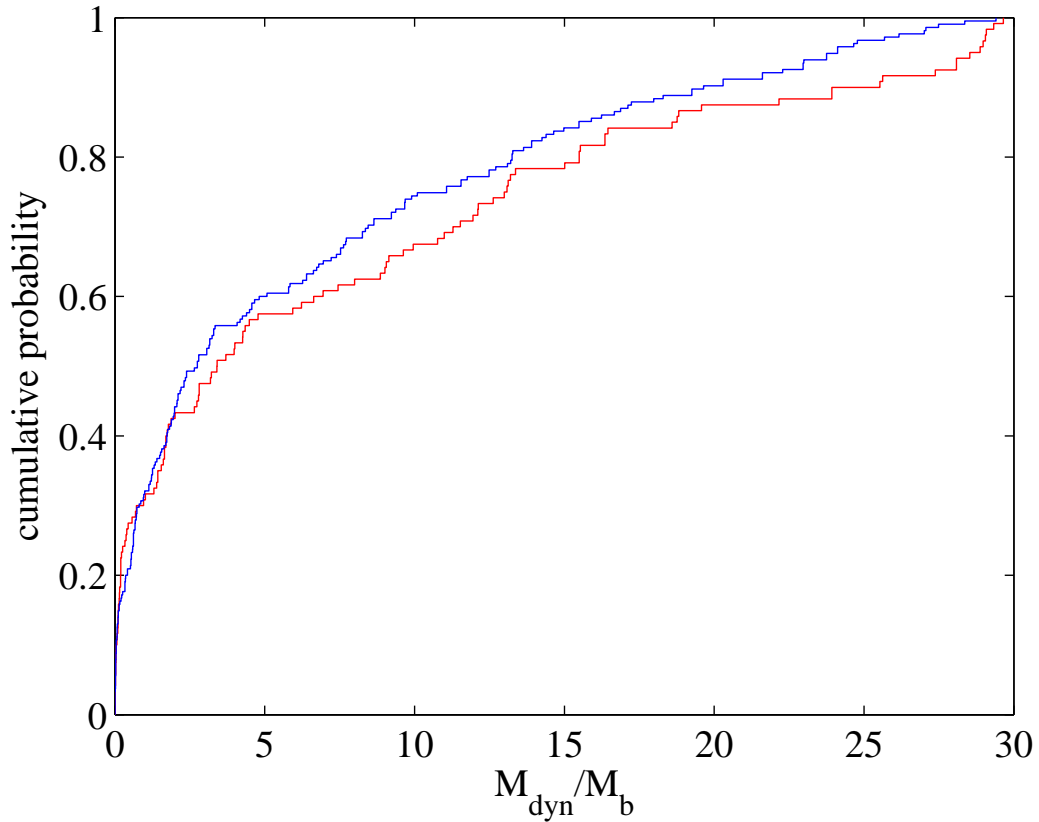


Figure 9. Probability distributions of M_{dyn}/M_b of ETGs and spiral galaxies using L17 M–L relation. The red and blue lines represent the distributions of the ETGs and spiral galaxies, respectively.

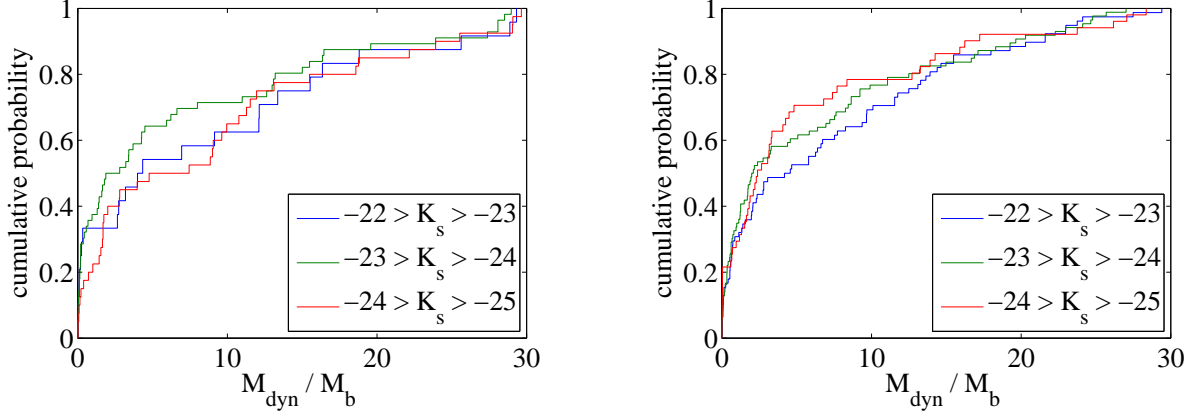


Figure 10. Probability distributions of M_{dyn}/M_b of the ETGs and spiral galaxies of different galaxy luminosities using L17 M–L relation. Left: M_{dyn}/M_b of ETGs. Right: M_{dyn}/M_b of spiral galaxies. The blue, green, and red lines represent the M_{dyn}/M_b distributions of the galaxies that had absolute magnitudes from -22 to -23 , -23 to -24 , and -24 to -25 , respectively.

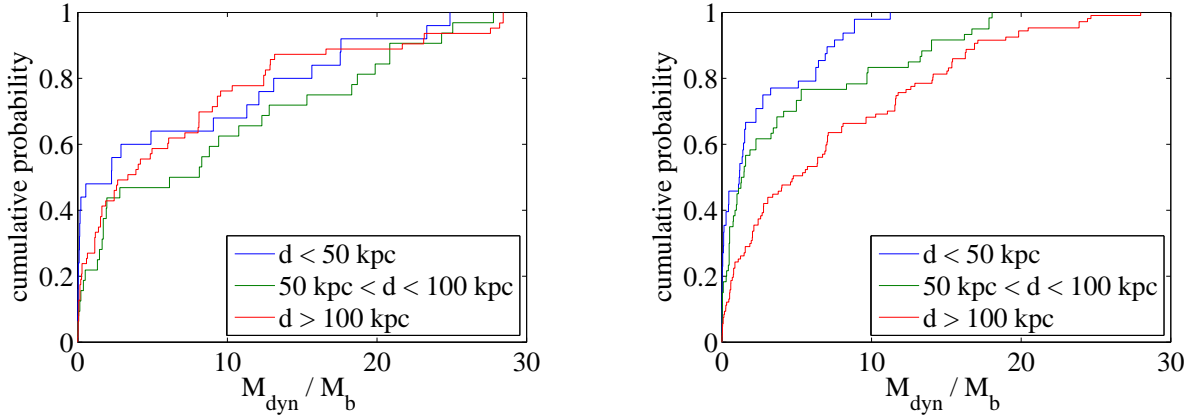


Figure 11. Probability distributions of M_{dyn}/M_b of the ETGs and spiral galaxies of different observed satellite-to-host galaxy distances using L17 M–L relation. Left: M_{dyn}/M_b of ETGs galaxies. Right: M_{dyn}/M_b of spiral galaxies. The blue, green, and red lines represent the M_{dyn}/M_b distributions for distances less than 50 kpc, between 50 kpc and 100 kpc, and greater than 100 kpc, respectively.

Table 2. Results of the K–S test of M_{dyn}/M_b in various observed satellite-to-host galaxy distances.

| | ETGs | | spiral | |
|--------------------------------|--------------|--------------------------------|--------------|--------------------------------|
| | $d < 50$ kpc | $50 \text{ kpc} < d < 100$ kpc | $d < 50$ kpc | $50 \text{ kpc} < d < 100$ kpc |
| $50 \text{ kpc} < d < 100$ kpc | 20% | – | 31% | – |
| $d > 100$ kpc | 39% | 36% | 0.18% | 2.8% |

APPENDIX

A. SIMULATION FOR OBSERVED MASS RATIO DISTRIBUTION

For a host galaxy with mass M_0 , a satellite galaxy at a circular orbit with distance d_0 to the host galaxy will have a rotation velocity v_0 :

$$v_0^2 = \frac{GM_0}{d_0}. \quad (\text{A1})$$

For an observer in a random position, the unit vector of the line-of-sight \vec{p} is related to the origin of the host galaxy with the following equations

$$\begin{aligned} p_x &= \cos \phi \sqrt{1 - p_z^2}, \\ p_y &= \sin \phi \sqrt{1 - p_z^2}, \\ p_z &= 2\mu - 1, \end{aligned} \quad (\text{A2})$$

where $\mu = \cos \theta$, ϕ and θ are the parameters of \vec{p} in the polar coordinate centred at the origin of the host galaxy. Figure 12 displayed a schematic of the line-of-sight and the host-satellite plane. The observed separate distance d_1 is the projected component perpendicular to the line-of-sight, and the observed velocity v_1 is the projected velocity along the line-of-sight. Assuming that the observed velocity square represents one-third of the true velocity square, the observed mass of the host galaxy M_1 has the following relationship to the true mass M_0

$$M_1 = \frac{3v_1^2 d_1}{G} = M_0 \frac{3v_1^2 d_1}{v_0^2 d_0}. \quad (\text{A3})$$

Therefore the maximum M_1 could be three M_0 in the case of the line-of-sight is parallel to the direction of \vec{v}_0 . For a host galaxy at the original point and a satellite orbit on the $x - y$ plane, d_1 and v_1 are functions of \vec{d} , \vec{v} and \vec{p} .

$$\begin{aligned} d_1 &= \sqrt{d_0^2 - (\vec{d}_0 \cdot \vec{p})^2}, \\ v_1 &= |\vec{v}_0 \cdot \vec{p}|. \end{aligned} \quad (\text{A4})$$

If we put a host galaxy with mass M_0 at the original point and a satellite at $(d_0, 0, 0)$ with initial velocity $(0, v, 0)$ where $v = kv_0$, we get a circular orbit for $k = 1$ and elliptical orbits for $0 < k < \sqrt{2}$ but $k \neq 1$. Moreover, the initial point would be the apocenter for $0 < k < 1$ and pericenter for $1 < k < \sqrt{2}$.

With the same ellipticities, we can have different d_0 and v_0 . We scaled real distance and velocity of the satellite to cd_0 and v/\sqrt{c} , respectively. The range of c in our simulation is showed in Table 3. We note that we have assumed the mass distribution of the host galaxy to be with the pericenter distance of the minima orbit of the satellite in this simulation.

In our study, we used five different k , which were all less than or equal to one. Therefore, the initial points are the apocenter points. We first used $M_0 = 10^{11} M_\odot$ (assuming $M_* = 10^{10} M_\odot$) and $d = 250$ kpc to simulate the positions and velocities of the satellite galaxy for the five orbits. For each orbit, we then randomly selected a position, a sight vector \vec{p} and a scaled parameter c to simulate an observation event. The parameters μ and ϕ are assumed to be uniformly distributed in $[0, 1]$

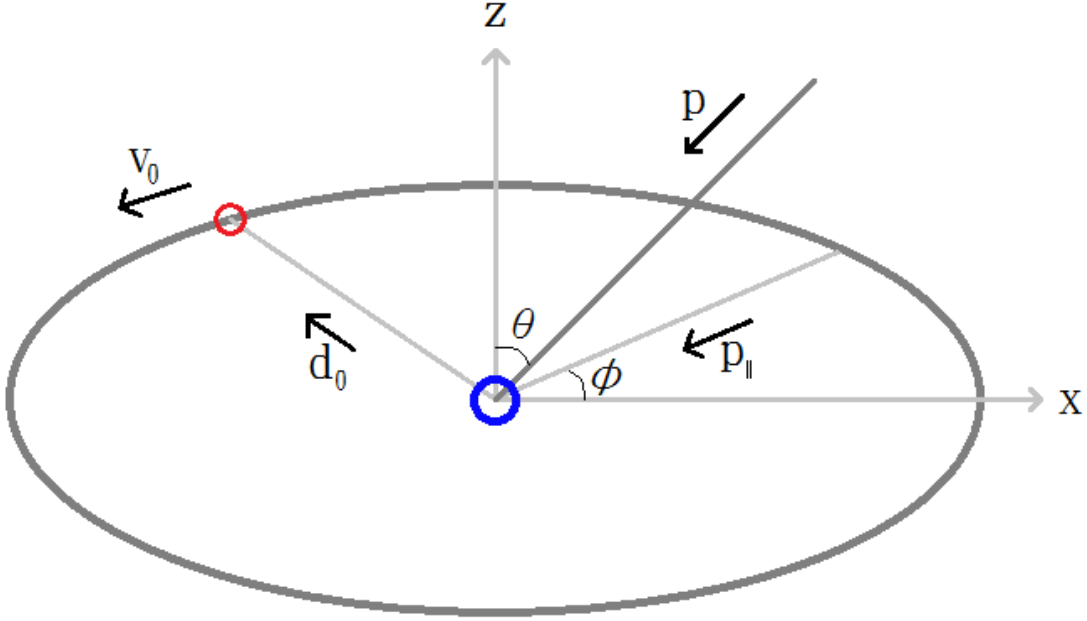


Figure 12. Schematic of the line-of-sight and the host-satellite plane. The blue and red circles represent the host and satellite galaxy, respectively. The z-axis is the rotation axis of the satellite galaxy. The direction of the real velocity is \vec{v}_0 , the real distance is \vec{d}_0 , the line-of-sight is \vec{p} , and the projecting component of \vec{p} on host-satellite plane is \vec{p}_{\parallel} . ϕ is the angle between x-axis and \vec{p}_{\parallel} ; θ is the angle between z-axis and \vec{p} .

and $[0, 2\pi]$, respectively. The observed d_1 and v_1 can be determined by the Equation A3, and the observed M_1 can be determined by the Equation A4. We simulated one million observation events for each orbit; the results are illustrated in Figure 5. Table 3 displayed the parameters for the five orbits which we used in this study.

Table 3. Parameters of the simulated orbits

| k | pericenter distance (kpc) | ϵ | range of c |
|-------|------------------------------|------------|--------------|
| 1 | 250 | 1 | [1/5, 1] |
| 0.943 | 200 | 0.8 | [1/4, 1] |
| 0.866 | 150 | 0.6 | [1/3, 1] |
| 0.756 | 100 | 0.4 | [1/2, 1] |
| 0.577 | 50 | 0.2 | [1, 1] |

REFERENCES

- Alabi, A. B., Forbes, D. A., Romanowsky, A. J., et al. 2016, *MNRAS*, 460, 3838
- Alabi, A. B., Forbes, D. A., Romanowsky, A. J., et al. 2017, *MNRAS*, 468, 3949
- Alam, S., Albareti, F. D., Allende Prieto, C., et al. 2015, *ApJS*, 219, 12
- Bell, E. F., McIntosh, D. H., Katz, N., & Weinberg, M. D. 2003, *ApJS*, 149, 289
- Bell, E. F., Naab, T., McIntosh, D. H., et al. 2006, *ApJ*, 640, 241
- Binney, J., & Tremaine, S. 2008, *Galactic Dynamics: Second Edition*
- Boardman, N. F., Weijmans, A.-M., van den Bosch, R., et al. 2016, *MNRAS*, 460, 3029
- Boselli, A., Cortese, L., Boquien, M., et al. 2014, *A&A*, 564, A66
- Bois, M., Bournaud, F., Emsellem, E., et al. 2010, *MNRAS*, 406, 2405
- Brainerd, T. G., & Specian, M. A. 2003, *ApJL*, 593, L7
- Bruzual, G., & Charlot, S. 2003, *MNRAS*, 344, 1000
- Campbell, D. J. R., Frenk, C. S., Jenkins, A., et al. 2017, *MNRAS*, 469, 2335
- Cappellari, M., McDermid, R. M., Alatalo, K., et al. 2012, *Nature*, 484, 485
- Cappellari, M., Scott, N., Alatalo, K., et al. 2013, *MNRAS*, 432, 1709
- Cappellari, M. 2016, *ARA&A*, 54, 597
- Cattaneo, A., Mamon, G. A., Warnick, K., & Knebe, A. 2011, *A&A*, 533, A5
- Chabrier, G. 2003, *ApJL*, 586, L133
- Chabrier, G. 2003, *PASP*, 115, 763
- Chen, C.-W., Côté, P., West, A. A., et al. 2010, *ApJS*, 191, 1
- Corbelli, E., & Salucci, P. 2000, *MNRAS*, 311, 441
- Conroy, C., Prada, F., Newman, J. A., et al. 2007, *ApJ*, 654, 153
- Courteau, S., Cappellari, M., de Jong, R. S., et al. 2014, *Reviews of Modern Physics*, 86, 47
- Courteau, S., & Dutton, A. A. 2015, *ApJL*, 801, L20
- Cox, T. J., Dutta, S. N., Di Matteo, T., et al. 2006, *ApJ*, 650, 791
- Crain, R. A., Schaye, J., Bower, R. G., et al. 2015, *MNRAS*, 450, 1937
- Dekel, A., Stoehr, F., Mamon, G. A., et al. 2005, *Nature*, 437, 707
- Di Paolo, C., Salucci, P., & Erkurt, A. 2019, *MNRAS*, 490, 5451
- Emsellem, E., Krajnovic, D., & Sarzi, M. 2014, *MNRAS*, 445, L79
- Faber, S. M., & Gallagher, J. S. 1979, *ARA&A*, 17, 135
- Forbes, D. A., Alabi, A., Romanowsky, A. J., et al. 2016, *MNRAS*, 458, L44
- Gavazzi, G., Pierini, D., & Boselli, A. 1996, *A&A*, 312, 397
- Graham, A. W., Janz, J., Penny, S. J., et al. 2017, *ApJ*, 840, 68
- Hansen, S. H., & Moore, B. 2006, *NewA*, 11, 333
- Haynes, M. P., Giovanelli, R., Kent, B. R., et al. 2018, *ApJ*, 861, 49
- Hills, J. G. 1975, *AJ*, 80, 809
- Into, T., & Portinari, L. 2013, *MNRAS*, 430, 2715
- Janz, J., Penny, S. J., Graham, A. W., et al. 2017, *MNRAS*, 468, 2850
- Jin, Y., Zhu, L., Long, R. J., et al. 2020, *MNRAS*, 491, 1690
- Karachentsev, I. D., Makarov, D. I., & Kaisina, E. I. 2013, *AJ*, 145, 101
- Kennicutt, R. C., Armus, L., Bendo, G., et al. 2003, *PASP*, 115, 928
- Khalil, S., & Muñoz, C. 2002, *Contemporary Physics*, 43, 51
- Kroupa, P. 1998, *Brown Dwarfs and Extrasolar Planets*, 483
- Kuno, N., Sato, N., Nakanishi, H., et al. 2007, *PASJ*, 59, 117
- Lane, R. R., Salinas, R., & Richtler, T. 2015, *A&A*, 574, A93
- Lange, J. U., van den Bosch, F. C., Zentner, A. R., et al. 2019, *MNRAS*, 482, 4824
- Lange, J. U., van den Bosch, F. C., Zentner, A. R., et al. 2019, *MNRAS*, 487, 3112
- Leroy, A. K., Walter, F., Brinks, E., et al. 2008, *AJ*, 136, 2782
- Li, S.-lin., Shi, Y., Chen, Y.-M., et al. 2018, *MNRAS*, 480, 1705
- Lim, S. H., Mo, H. J., Lu, Y., et al. 2017, *MNRAS*, 470, 2982
- Martig, M., Bournaud, F., Teyssier, R., et al. 2009, *ApJ*, 707, 250
- McAlpine, S., Helly, J. C., Schaller, M., et al. 2016, *Astronomy and Computing*, 15, 72

- McGaugh, S. S., & Schombert, J. M. 2014, *AJ*, 148, 77
- McGaugh, S. S., & Schombert, J. M. 2015, *ApJ*, 802, 18
- Milgrom, M., & Sanders, R. H. 2003, *ApJL*, 599, L25
- McKay, T. A., Sheldon, E. S., Johnston, D., et al. 2002, *ApJL*, 571, L85
- More, S., van den Bosch, F. C., Cacciato, M., et al. 2011, *MNRAS*, 410, 210
- Navarro, J. F., Frenk, C. S., & White, S. D. M. 1996, *ApJ*, 462, 563
- Nigoche-Netro, A., Ruelas-Mayorga, A., Lagos, P., et al. 2015, *MNRAS*, 446, 85
- Nigoche-Netro, A., Ramos-Larios, G., Lagos, P., et al. 2016, *MNRAS*, 462, 951
- Nigoche-Netro, A., Ramos-Larios, G., Lagos, P., et al. 2019, *MNRAS*, 488, 1320
- Ostriker, J. P., & Peebles, P. J. E. 1973, *ApJ*, 186, 467
- Roberts, M. S., & Whitehurst, R. N. 1975, *ApJ*, 201, 327
- Romanowsky, A. J., Douglas, N. G., Arnaboldi, M., et al. 2003, *Science*, 301, 1696
- Penoyre, Z., Moster, B. P., Sijacki, D., et al. 2017, *MNRAS*, 468, 3883
- Portinari, L., Sommer-Larsen, J., & Tantalo, R. 2004, *MNRAS*, 347, 691
- Prada, F., Vitvitska, M., Klypin, A., et al. 2003, *ApJ*, 598, 260
- Rubin, V. C., & Ford, W. K., Jr. 1970, *ApJ*, 159, 379
- Rubin, V. C. 1983, *Science*, 220, 1339
- Ruff, A. J., Gavazzi, R., Marshall, P. J., et al. 2011, *ApJ*, 727, 96
- Sanders, R. H. 2014, *MNRAS*, 439, 1781
- Schaye, J., Crain, R. A., Bower, R. G., et al. 2015, *MNRAS*, 446, 521
- Sofue, Y. 2012, *PASJ*, 64, 75
- Toloba, E., Boselli, A., Cenarro, A. J., et al. 2011, *A&A*, 526, A114
- Tully, R. B., Rizzi, L., Shaya, E. J., et al. 2009, *AJ*, 138, 323
- Tully, R. B. 2015, *AJ*, 149, 171
- Tully, R. B., Courtois, H. M., & Sorce, J. G. 2016, *AJ*, 152, 50
- van de Ven, G., Falcón-Barroso, J., McDermid, R. M., et al. 2010, *ApJ*, 719, 1481
- Wojtak, R., & Mamon, G. A. 2013, *MNRAS*, 428, 2407
- Young, J. S., Xie, S., Kenney, J. D. P., et al. 1989, *ApJS*, 70, 699
- Zibetti, S., Charlot, S., & Rix, H.-W. 2009, *MNRAS*, 400, 1181
- Zwicky, F. 1937, *ApJ*, 86, 217